A Green Desulfurization Technique: Utilization of Flue Gas SO$_2$ to Produce H$_2$ via a Photoelectrochemical Process Based on Mo-Doped BiVO$_4$

Jin Han [†], Kejian Li [†], Hanyun Cheng and Liwu Zhang*

Shanghai Key Laboratory of Atmospheric Particle Pollution and Prevention, Department of Environmental Science and Engineering, Fudan University, Shanghai, China

A green photoelectrochemical (PEC) process with simultaneous SO$_2$ removal and H$_2$ production has attracted an increasing attention. The proposed process uses flue gas SO$_2$ to improve H$_2$ production. The improvement of the efficiency of this process is necessary before it can become industrial viable. Herein, we reported a Mo modified BiVO$_4$ photocatalysts for a simultaneous SO$_2$ removal and H$_2$ production. And the PEC performance could be significantly improved with doping and flue gas removal. The evolution rate of H$_2$ and removal of SO$_2$ could be enhanced by almost three times after Mo doping as compared with pristine BiVO$_4$. The enhanced H$_2$ production and SO$_2$ removal is attributed to the improved bulk charge carrier transportation after Mo doping, and greatly enhanced oxidation reaction kinetics on the photoanode due to the formation of SO$_3^{2-}$ after SO$_2$ absorption by the electrolyte. Due to the utilization of SO$_2$ to improve the production of H$_2$, the proposed PEC process may become a profitable desulfurization technique.

Keywords: hydrogen, sulfur dioxide, solar energy, Photoelectrochemical (PEC), Mo-doped BiVO$_4$

INTRODUCTION

Sulfur dioxide (SO$_2$), as one of the acid gases, could transform into some atmospheric products (e.g., sulfate, sulfuric acid aerosol) through the chemical process in the atmosphere. It and its atmospheric products are detrimental to human health, and cause lots of environmental problems such as smog formation, acid deposition, and degradation of visibility. As is well-known, the SO$_2$ mainly enters the atmosphere through the anthropogenic processes, e.g., combustion and release of petroleum, fossil fuel, etc. (Lelieveld and Heintzenberg, 1992; McDonald-Buller et al., 2016). Till now, to remove SO$_2$ released from the burning of fossil fuels, several effective methods has been developed (Srinivasan and Grutzeck, 1999; Bashikova et al., 2001; Xia et al., 2011; Kaplan et al., 2013; Yang et al., 2013). Among these technologies, Wet Flue Gas Desulfurization (WFGD) has been one of the state-of-the-art technologies for SO$_2$ removal with high efficiency, simple equipment and obtaining multi-useful byproducts (Yang et al., 2012; Lu et al., 2013). Unfortunately, there are some inevitable drawbacks with the WFGD process: for example, the oxidation process energy of SO$_3^{2-}$ to final SO$_4^{2-}$ is wasted and it is not consistent with the sustainable principles. In order to solve this problem, our group proposed a solar-to-H$_2$ energy conversion with SO$_2$ removal

simultaneously via a solar water splitting process for the first time (Han et al., 2017). Since the oxidation of SO$_3^{2-}$ (formed during desulfurization process) needs much lower activation energy and 2 electrons than that of water, acted as a sacrificing reagent during the process, thus it could significantly improve the evolution rate of H$_2$. This method not only utilizes the waste energy during the desulfurization process, also realizes the energy production by using air pollutants, which could achieve the zero release of SO$_2$.

Though we have reported a photoresponse semiconductor (BiVO$_4$) for H$_2$ generation with SO$_2$ removal, but it is still a challenge to facilitate the performance due to the intrinsic low mobility of photogenerated charges of BiVO$_4$. Lots of methods have been proposed to solve this problem, such as controlling the morphology (McDonald and Choi, 2012; Kim and Choi, 2014; Zhou et al., 2014), metal and nonmetal doping (Jo et al., 2012; Chen et al., 2015; Huang H. et al., 2015; Huang H. W. et al., 2015; Huang et al., 2017), forming heterojunctions (Hong et al., 2011; Luo et al., 2011; Seabold and Choi, 2012; Zhang et al., 2016). These modifications have improved the properties of BiVO$_4$ greatly by reducing the band-gap energy or improving the charge carrier transport. It has been reported that Mo^{6+} ion substitute the V site in monoclinic sheelite BiVO$_4$ could improve the photoinduced carriers, which could facilitate the oxidation while in water splitting reaction system theoretically and experimentally (Luo et al., 2011, 2013; Parmar et al., 2012; Ding et al., 2014; Park et al., 2014; Seabold et al., 2014; Zhou et al., 2014; Jiang et al., 2015, 2017; Kuang et al., 2016; Nair et al., 2016; Pattengale and Huang, 2016). However, Mo-doped BiVO$_4$ has not been studied as photoanode for flue gas SO$_2$ removal. Here, we prepared Mo-doped BiVO$_4$ for enhancing H$_2$ generation with simultaneous SO$_2$ removal. Moreover, the importance of the amount of Mo-dopants on the performance of BiVO$_4$ with SO$_2$ removal was also studied. Besides we prepared a series of Mo-doped BiVO$_4$ films with different content. The structure characterizations of the obtained films are investigated by XRD, SEM, Raman, UV-vis. Furthermore, we studied the performance of H$_2$ generation and efficiency of SO$_2$ removal.

EXPERIMENT

Synthesis of the Catalysts

In this work, the deionized water (DI water) was used throughout the whole experiment, and all the chemical reagents are analytical grade and used without any further purification.

F-doped SnO$_2$ coated glass (FTO) were purchased from China Southern Glass Co. Ltd, and the FTO glasses were sonicated by immersing in acetone, ethanol and DI water for removing the impurities on the surface of the glass. For comparison, the pristine BiVO$_4$ was also prepared. All of the electrodes were synthesized by drop-coating method. The precursor solution was dropped onto the conducting side of FTO, followed by annealing in air. The precursor solutions were synthesized by the following procedure (Zhang et al., 2014): diethylene-etriaminepentaacetic acid (DTPA) and ammonia in water (13.0 mol L^{-1}) were added into hot deionized water. After dissolution, the stoichiometric Bi(NO$_3$)$_3$•5H$_2$O, V$_2$O$_5$ powder and moderate ammonium molybdate tetrahydrate (H$_{24}$Mo$_7$N$_6$O$_{24}$·4H$_2$O) were added into

sequence as listed. The resulted mixture was stirred and heated for an hour to promote the dissolution and reaction (complexation of Bi^{3+}, V^{5+}, and Mo^{6+} with DTPA) until the mixture turned into a transparent solution. Here, we prepared three different samples with the content of Mo ranging from 1, 3, to 5. The amounts of doped Mo were 1 atom%, 3 atom%, 5 atom%, and were denoted as BiVO$_4$(Mo-1), BiVO$_4$(Mo-3), BiVO$_4$(Mo-5), respectively. Then, 40 μl prepared solutions were dropped onto the conducting side of FTO (1 × 2 cm) respectively. After dried at 60° C in oven, the films were annealed at 500° C for 3 h with a ramping rate of 2° C min^{-1} in air. The above process was repeated by three times for the synthesis of the electrode.

Characterization of the Samples

The crystal structures of the as-prepared samples were determined using an X-Ray Diffraction (XRD) with Cu Kα radiation ranging from 10 to 60°. The crystallite sizes of the samples were calculated using the Scherrer formula:

$$D = \frac{K\lambda}{\beta \cos\theta} \tag{1}$$

Where D is the average crystallite size (nm), λ is the wavelength of the X-ray radiation (0.154 nm), K is the shape factor (0.9), β is the peak width at half-maximum height, corrected for instrumental broadening, and 2θ = 28.7°. The micromorphology and the microstructure of the samples were determined by using field emission scanning electron microscopy (FE-SEM, Hitachi S-4800, Japan). UV-vis transmission spectra of the as-prepared catalysts were measured using a UV-Vis spectrophotometer (SHIMADZU UV-2600) with an integrating sphere attachment. BaSO$_4$ used as a standard. Raman spectra were recorded with a Raman spectrometer (HORIBA, X-plo RA Plus), a green laser (532 nm) were used as excitation sources.

PEC Measurement

The apparatus for the PEC tests was a gastight photoreactor. The PEC performance were conducted with a typical three-electrode configuration by using a potentiostat (CHI 660E, Shanghai Chenhua Co. Lid. China). The synthesized pure BiVO$_4$ or Mo-doped BiVO$_4$ electrode was used as working electrode, Pt wire was used as counter electrode and Hg/HgO electrode was used as reference electrode. The electrolyte solutions for the PEC tests were prepared by absorbing SO$_2$ gas with NaOH solutions of certain concentration (detailed in **Table 1**). We bubbled SO$_2$ of concentration is 1,000 ppm successively to NaOH aqueous with the flow rate of 200 ml min^{-1} to form Na$_2$SO$_3$ with a specific concentration. Eventually, the obtained electrolytes for PEC tests were 0.1 M NaOH−0.025 M Na$_2$SO$_3$ [denoted as NaOH(aq)+SO$_2$(g)-1], 0.1 M NaOH-0.05 M Na$_2$SO$_3$ [denoted as NaOH(aq)+SO$_2$(g)-2], 0.1 M NaOH-0.075 M Na$_2$SO$_3$ [denoted as NaOH(aq)+SO$_2$(g)-3]. For comparison, the NaOH (aq, 0.1 M) solution was also prepared. The PEC tests were measured under illumination by using a 300 W Xe lamp solar simulator with AM 1.5 G filter (100 mW cm^{-2}) from the back side of the working electrode, as well as in dark conditions. Liner Sweep Voltammetry (LSV) was measured with the sweep rate of 10 mV s^{-1}.

The structures of prepared BiVO$_4$ and Mo-doped BiVO$_4$ bulk were optimized by using the CASTEP code (Ding et al., 2014). The primitive cell of pure monoclinic sheelite BiVO$_4$ was relaxed using 400 eV energy cut off for the plane-wave expansion. The structural model of Mo-doped monoclinic sheelite BiVO$_4$ was built by substituting one V atom in a relaxed ($2 \times 1 \times 2$) supercell of monoclinic sheelite BiVO$_4$ with one Mo atom.

Hydrogen Evolution

The reactor for hydrogen evolution experiments is identical with the apparatus used for PEC tests, which use a two-electrode configuration. The electrolyte was NaOH solution bubbled with SO$_2$ gas. The experiments were conducted under illumination

TABLE 1 | The detailed information of electrolyte and SO$_2$ absorbing efficiency.

Items	NaOH(aq)-SO$_2$(g)-1	NaOH(aq)-SO$_2$(g)-2	NaOH(aq)-SO$_2$(g)-3
Concentration of NaOH/M	0.150	0.200	0.250
Concentration of SO$_2$/ppm	1,000	1,000	1,000
SO$_2$ flow rate/ml min^{-1}	200	200	200
SO$_2$ inletting time/min	112	224	336
Resulted concentration of SO$_3^{2-}$/M	~0.025	~0.050	~0.075
SO$_2$ absorbing efficiency/%	~99	~98	~98

using a 300 W Xe lamp with AM 1.5 G filter (100 mW cm^{-2}) from the back side of the photoanodes in a 150 ml reactor with 100 ml electrolytes filled in and the external bias was 1.6 V. The amount of H$_2$ was analyzed by gas chromatography using a thermal conduction detector (TCD) once an hour. The pH values of the solution during the PEC tests were detected by Ohaus (STARTER 2100). The theoretical evolution rate of H$_2$ is calculated according to the following equation:

$$v = \frac{I \times t}{Z \times F \times A \times 3600} \tag{2}$$

Where, v indicates the evolution rate of H$_2$ (mol cm^{-2} h^{-1}); I indicates the average current (A); t indicates the time (s); Z indicates the transferred electron number (1); F is the Faraday's constant (96,500 C mol^{-1}); A is the area of the film (cm^2).
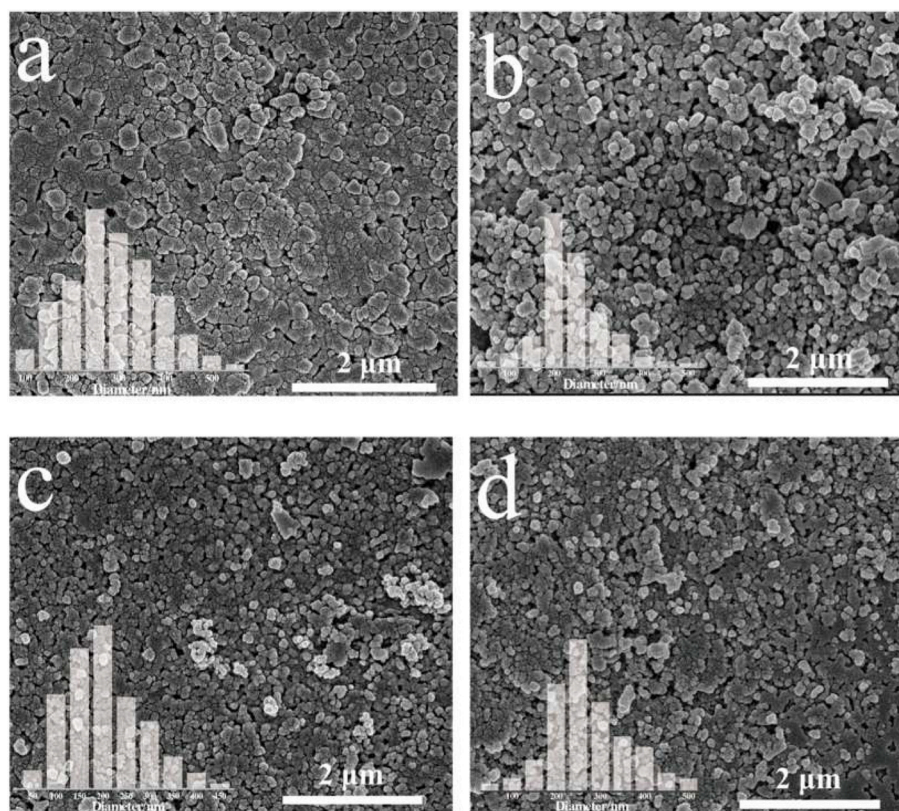
The equation for the calculation of Faradaic efficiency is:

$$Faradaic\ efficiency\ (\%) = \frac{m \times n \times F}{I \times t} \times 100\% \tag{3}$$

Where, m is the experimental value of H$_2$ (mol); n is the reacted electron number (1); F is the Faraday's constant (96,500 C mol^{-1}); I is the average current (A); t is the time (s).

FIGURE 1 | SEM images and particle range of **(a)** pure BiVO$_4$; **(b)** BiVO$_4$(Mo-1); **(c)** BiVO$_4$(Mo-3); **(d)** BiVO$_4$(Mo-5).

RESULTS AND DISCUSSION

## Structure and Physical Properties of the Photoelectrode

The SEM (Scanning Electron Microscopy) images of pristine BiVO$_4$ and Mo-doped BiVO$_4$ films are shown in **Figure 1**. All of the films present nanoparticle structure while a rougher, more disordered structure can be observed in the BiVO$_4$ films. Besides, the incorporation of Mo could decrease the average size of BiVO$_4$ with decreasing aggregation of the particles. The average diameter of pure BiVO$_4$ is about 280 nm (**Figure 1a**), and the average diameter of Mo-doped BiVO$_4$ are ranging from 200 to 250 nm, which are smaller than that of pure BiVO$_4$ (**Figures 1b–d**). Besides, the smaller particle size of the as-prepared photocatalyst could provide more available active sites, which could be in favor of the PEC performance.

Figure 2A compares the XRD (X-Ray Diffraction) patterns of pure and Mo-doped BiVO$_4$ films with different concentrations of Mo dopant. All the diffraction peaks are assigned to phase-pure monoclinic sheelite BiVO$_4$ structure (JCPDS No. 14-0688). Since the films are very thin, the diffraction peaks of FTO substrate are also observed in XRD. No noticeable peaks of MoO$_3$ is detected in the Mo-doped BiVO$_4$, the results are consistent with previous study (Berglund et al., 2012; Luo et al., 2013; Chen et al., 2015; Nair et al., 2016; Thalluri et al., 2016). Additionally, the main
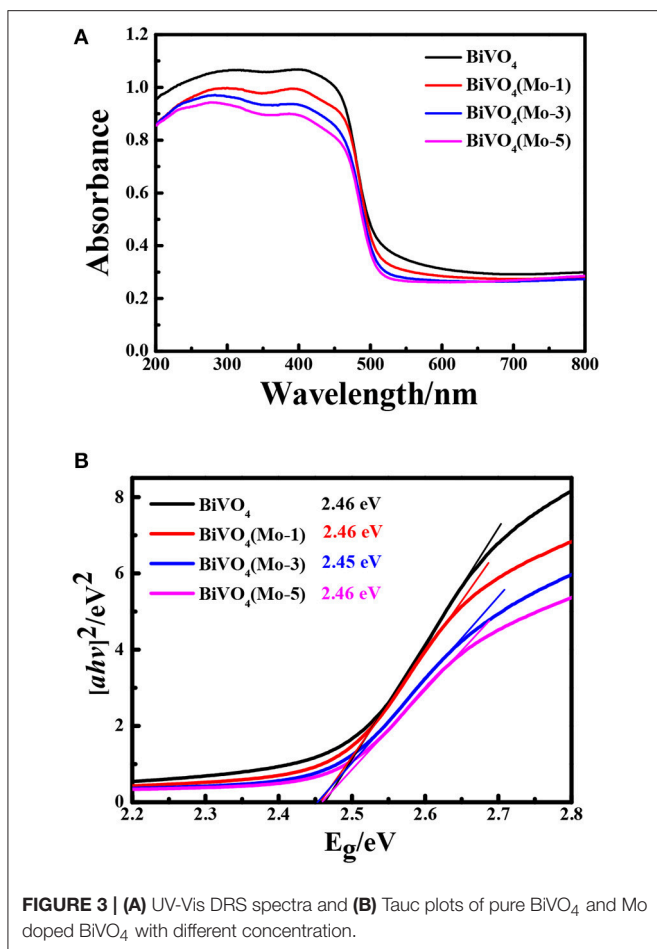
peaks of the monoclinic BiVO$_4$ structure shift to lower intensity and higher scattering angles in the Mo-doped BiVO$_4$ films since the radius of Mo is higher than that of V. This represents a shrinkage or an enlargement of the d spacing of corresponding crystal planes due to incorporation of dopant cations into V sites of BiVO$_4$ (Parmar et al., 2012). As the pure phase and modification in d spacing, it can be calculated that the Mo have been effectively incorporated into the crystal lattice of BiVO$_4$ with the monoclinic phase unchanged (Parmar et al., 2012). Furthermore, the crystallite sizes calculated by using the Scherrer formula are 110, 117, 83, 85 nm for the BiVO$_4$, BiVO$_4$(Mo-1), BiVO$_4$(Mo-3), BiVO$_4$(Mo-5), respectively.

Though XRD shows some trace that Mo have been doped in the crystal of pure BiVO$_4$. However, it is too rough to identify the doping sites in the crystal lattice because of the low doping concentration. To probe the doping sites and local distortions of Mo-doped BiVO$_4$, the Raman spectra were measured and the results are shown in **Figure 2B**. The Raman mode located at 829 cm^{-1} is assigned to the symmetric stretching mode of VO$_4^{3-}$ units. It is clear that the symmetric stretching mode in Mo-doped BiVO$_4$ shifts to a lower wave number, which suggests Mo^{6+} substitutes V^{5+} in the VO$_4^{3-}$ tetrahedron (Luo et al., 2013; Zhang et al., 2014).

Optical properties of the films are very important for the PEC performance. **Figure 3A** displays the UV-Vis DRS absorption
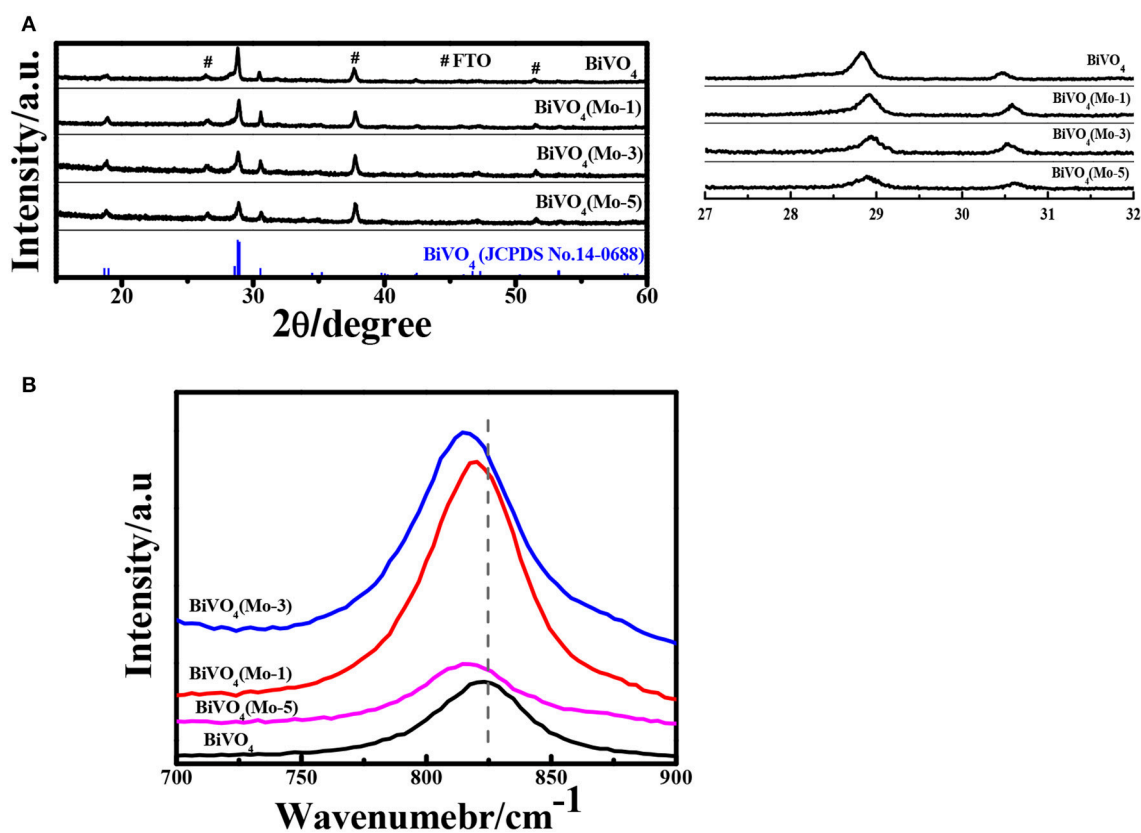
FIGURE 2 | (A) XRD patterns; (#: FTO) **(B)** Raman spectra of pure BiVO$_4$ and Mo doped BiVO$_4$ with different concentration.

FIGURE 3 | (A) UV-Vis DRS spectra and **(B)** Tauc plots of pure BiVO$_4$ and Mo doped BiVO$_4$ with different concentration.

FIGURE 4 | Linear Sweep Voltammograms (LSV) curves **(A)** BiVO$_4$(Mo-3) in different electrolyte systems; **(B)** different photoanodes in NaOH(aq)+SO$_2$(g)-3 electrolyte. (Scan speed: 10 mV s^{-1}).

spectra of the four films. All of the films present a strong absorption in the UV-Vis range, and the incorporation of Mo can hardly affect the absorption edges of BiVO$_4$. Besides, there isn't any peak shift in the UV-Vis spectra of Mo-doped films, which indicates there is not existence of the phase transfer from monoclinic to tetragonal structures with doping of Mo (**Figure 3A**; Pattengale and Huang, 2016). As the pure BiVO$_4$ shows a larger optical absorbance at wavelengths (>325 nm), thus the pure BiVO$_4$ are less porous than the Mo-doped BiVO$_4$ (Nair et al., 2016).

The optical band gap energy can be calculated by the following equation:

$$\alpha h\nu = A(h\nu - E_g)^{n/2} \qquad (4)$$

where, α, $h\nu$, A, and E_g are the absorption coefficient, photo energy, constant and band gap energy, respectively. The value of n depends on whether the transition is direct ($n = 1$) or indirect ($n = 4$). The bandgap of all the films are about 2.5 eV (**Figure 3B**), which is consistent with the reported band gap of BiVO$_4$ (Zhang et al., 2014). This result indicates that the incorporation of low amount of Mo could hardly influence the bandgap of BiVO$_4$, and it is considered to be the characteristic band gap of monoclinic phase of BiVO$_4$.
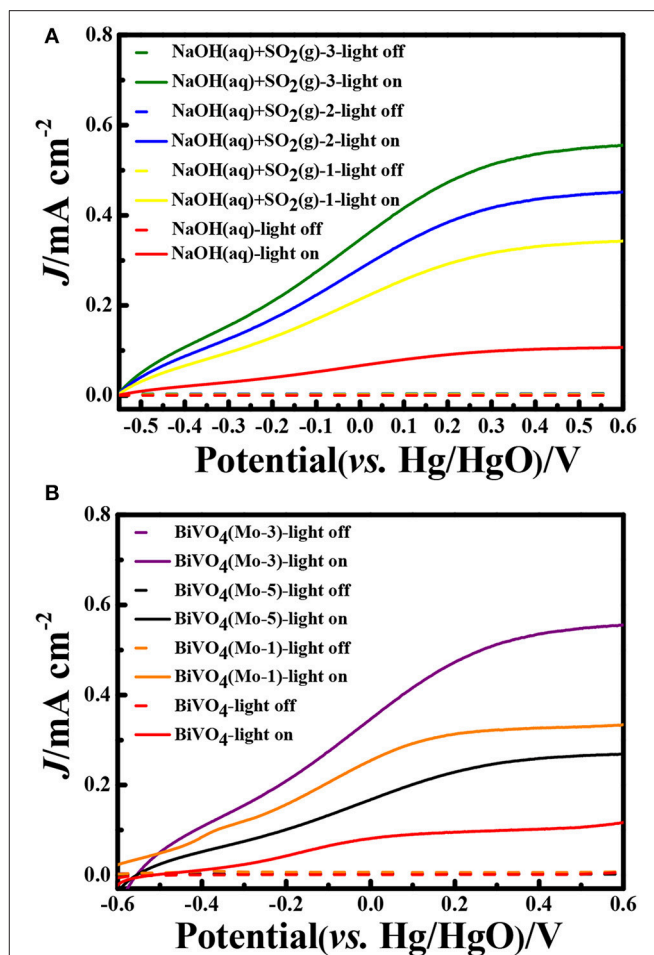
In the experiments, the SO$_2$ gas was absorbed by NaOH solutions and the concentration of SO$_3^{2-}$ was detected. Through analyzing, the removal efficiencies of SO$_2$ gas were about 98%, it indicated that the absorption method could removal SO$_2$ completely. In order to determine the PEC properties of the photoelectrodes, the Linear Sweep Voltammograms (LSV) were measured both in dark and under AM 1.5 G illumination (100 mW cm^{-2}; **Figure 4**). After analyzing the photocurrent densities of the photoanodes in different electrolyte systems after absorbing SO$_2$ (**Figure 4A**), it is concluded: (1) the photocurrent densities are negligible under dark conditions in different electrolyte systems; (2) the photocurrent densities could be significantly enhanced after inletting SO$_2$ into electrolyte. Since the introduction of SO$_2$ into electrolyte, the concentration of SO$_3^{2-}$ could be increased, and the oxidation reaction of SO$_3^{2-}$ needs lower activation energy and kinetically faster than that of water, thus the formed SO$_3^{2-}$ consumes the photogenerated holes instantaneously and generates a higher photocurrent density than that of water. Though the doping of Mo could decrease the light-absorbing slightly (**Figure 3A**), but it could

significantly enhance the bulk charge carrier transportation of $BiVO_4$. Therefore, the PEC performance of Mo-doping $BiVO_4$ is higher than that of $BiVO_4$. The photocurrent density is greatly dependent on the amount of SO_2 absorbed in the electrolyte. In NaOH(aq)+SO_2(g)-3, the photocurrent density is improved by 1.2 times, 1.6 times, and 5 times than that of NaOH(aq)+SO_2(g)-2, NaOH(aq)+SO_2(g)-1, NaOH(aq) at 0.5 V vs. Hg/HgO, respectively. The photocurrent density is significantly improved by 5 times as compared with our previous research on porous $BiVO_4$ (Han et al., 2017).

Compared with the four different electrode films in NaOH(aq)+SO_2(g)-3 electrolyte, it is clear that $BiVO_4$(Mo-3) displayed an outstanding PEC performance. The photocurrent density of $BiVO_4$(Mo-3) is 1.7 times than that of $BiVO_4$(Mo-1), 2 times than that of $BiVO_4$(Mo-5), and 5 times than that of $BiVO_4$ at 0.5 V vs. Hg/HgO (**Figure 4B**). The current densities of $BiVO_4$(Mo-3) in NaOH(aq) with and without SO_2(g)-3 at 0.6 V vs. Hg/HgO are ca. 0.6 and 0.1 mA cm^{-2}, respectively; the current density in NaOH(aq)+SO_2(g)-3 is 6 times higher than that in NaOH(aq). On the other hand, the evolution rate of H_2 in NaOH(aq)+SO_2(g)-3 (39.4 μmol h^{-1} cm^{-2}) is more than 40 times higher than that in NaOH (0.92 μmol h^{-1} cm^{-2}) in the **Table 2**. The above results indicate that the amount of Mo at 3 atom% could be an optimal choice.

The experiments for H_2 evolution in different systems were measured with a two-electrode configuration at a bias of 1.6 V under AM 1.5G irradiation. **Figure 5A** shows the amount of H_2 evolved in different systems and **Table 2** summarized the data of current densities, theoretical/ experimental evolution rates of H_2 and the Faradaic efficiencies in the different systems. Comparing each photoanodes in different solution systems, it is clear that the SO_2 removal could significantly facilitate the current density and evolution rate of H_2, which is in good agreement with our previous research (Han et al., 2017). Besides, the current density and evolution rates for $BiVO_4$(Mo-1, 3, 5) under light irradiation are higher than that under the dark condition. Furthermore, all of the Mo doped $BiVO_4$ photoanodes show more attractive performance than that of pure $BiVO_4$, and the $BiVO_4$(Mo-3) performed the best H_2 generation activities. As calculated, a highest H_2 evolution rate of 39.4 μmol h^{-1} cm^{-2} is realized in NaOH(aq)+SO_2(g)-3 with $BiVO_4$(Mo-3) as photoanode, and the H_2 evolution rate is only 0.19 μmol h^{-1} cm^{-2} in NaOH(aq) with the $BiVO_4$ as photoanode, suggesting the H_2 production

can be enhanced about 200 times with the removal of SO_2 simultaneously with 3 atom% Mo-doped $BiVO_4$. Furthermore, the theoretical evolution rates of H_2 are close to theoretical rates in each system, indicating a high Faradaic efficiency of H_2 production (higher than 95%). Besides, the catalysts could not dissolve although the solution is a strong basic aqueous solution.
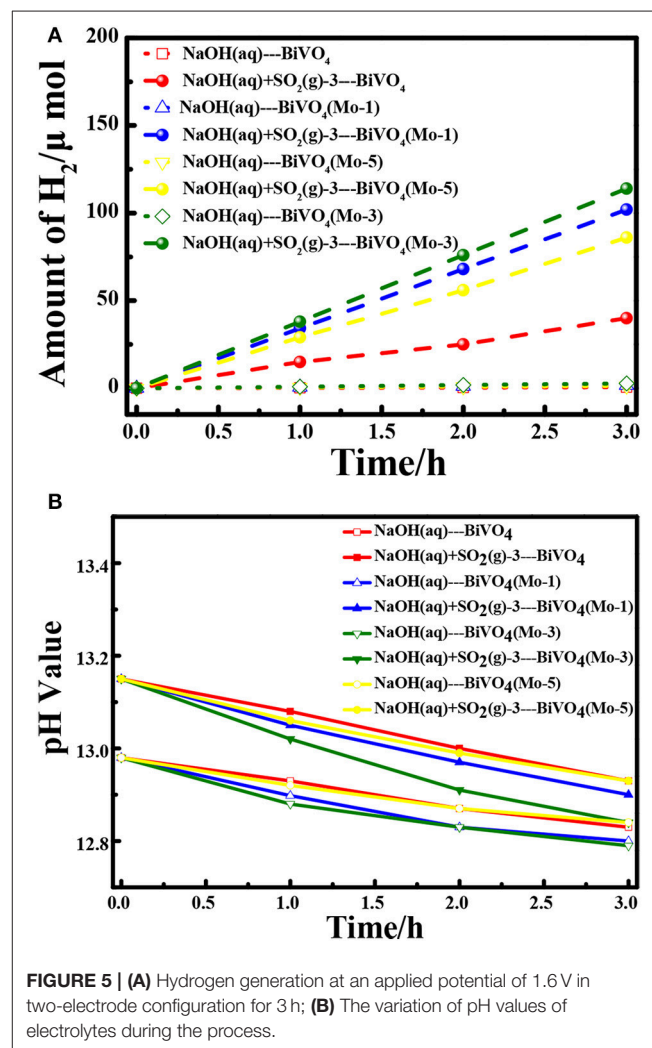

FIGURE 5 | (A) Hydrogen generation at an applied potential of 1.6 V in two-electrode configuration for 3 h; **(B)** The variation of pH values of electrolytes during the process.

TABLE 2 | The current density, theoretical and experimental evolution rate of H_2, and the Faradaic efficiency in different electrolytes [A—0.1 M NaOH; B—NaOH(aq)+SO_2(g)-3].

| Items	$BiVO_4$		$BiVO_4$(Mo-1)			$BiVO_4$(Mo-3)			$BiVO_4$(Mo-5)		
	A	B	A		B	A		B	A		B
	L	L	D	L	L	D	L	L	D	L	L
Current density/mA cm^{-2}	0.01	0.8	0.005	0.03	1.85	0.007	0.05	2.1	0.004	0.023	1.6
Theoretical evolution rate of H_2/μmol h^{-1} cm^{-2}	0.19	14.8	0.092	0.55	34.2	0.13	0.92	39.4	0.075	0.43	29.6
Experimental evolution rate of H_2/μmol h^{-1} cm^{-2}	0.18	14.4	0.088	0.54	33.7	0.126	0.90	38.8	0.071	0.41	29.2
Faradaic efficiency/%	95	97	96	98	99	97	98	98	95	95	99

In order to better understand the structure reconstruction with/without Mo doping, the geometric structures of pristine and the Mo-doped $BiVO_4$ were compared in **Figure 6**. It is clear that the doping of Mo could increase the length of Bi-O bonds. This phenomenon indicates that the original coordinated O atoms are "shifted" toward the doped Mo sites, and introduce "oxygen vacancies." As well-known, the oxygen vacancies could play an important role in improving the photocatalytic performance. Besides, the Mo^{6+} ion substitute the V site in monoclinic sheelite $BiVO_4$ could improve the transportation of photoinduced carriers, which could facilitate the charge carrier separation and leads to suppressed bulk recombination (Ding et al., 2014). Therefore, the photocatalytic activity is enhanced significantly after Mo-doping, as shown in **Figure 4**.

With the existence of flue gas SO_2 removal, SO_3^{2-} was formed in electrolyte solution. Then the photo-generated holes could be more quickly consumed by the formed SO_3^{2-} than that without

SO_3^{2-} (pure NaOH solution), because oxidation of SO_3^{2-} has a much lower activation energy and kinetically much faster than water oxidation or OH^- oxidation (McDonald and Choi, 2012; Seabold and Choi, 2012). The oxidation of SO_2 is thus proposed to replace the oxygen evolution reaction in water splitting, which can improve the water splitting efficiency and reduce the cost of H_2 production. The whole process for SO_2 removal with simultaneous production of H_2 is thus summarized and illustrated in **Figure 7**. Mo-doped $BiVO_4$ is first excited to generate e^- in conduction band (CB) and create hole (h^+) in the valence band (VB) at the same time. With the assistance of space charge layer and extra bias, the e^- transfer to the cathode and participate in cathode reaction for H_2 production. While the formed of SO_3^{2-} after flue gas SO_2 absorption is oxidized by the holes on the photoanode. As the Mo incorporated in $BiVO_4$ could improve the electronic conductivity of pure $BiVO_4$ (Luo et al., 2011; Pilli et al., 2011), therefore, the e^- produced in Mo doped
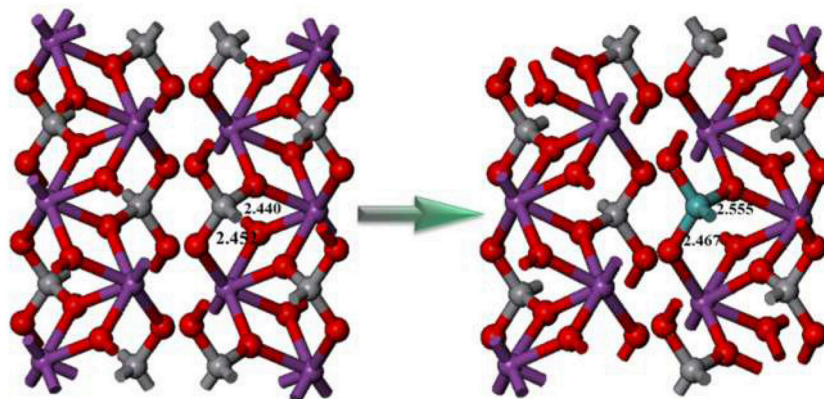

FIGURE 6 | The conventional cell of pure monoclinic sheelite $BiVO_4$ **(left)** and supercell of Mo doped monoclinic sheelite $BiVO_4$ **(right)**.
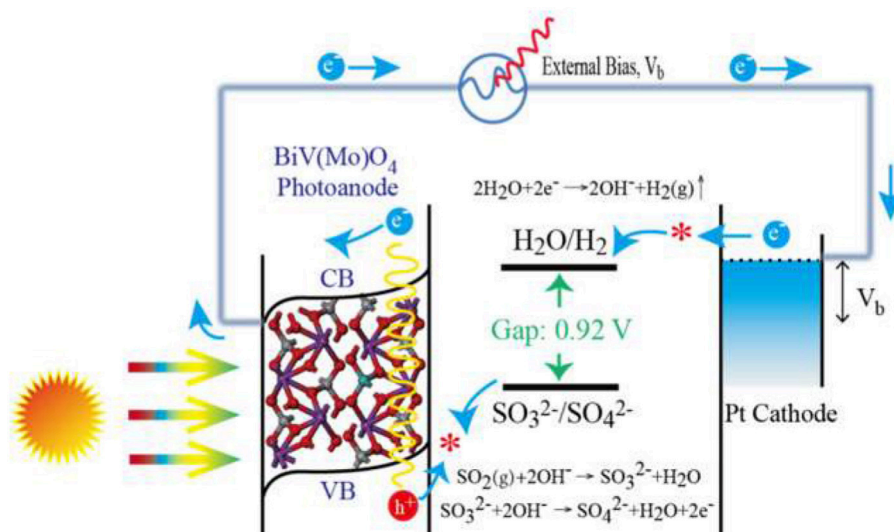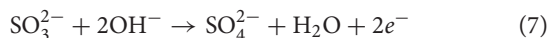

**FIGURE 7 |** Schematic illustration of H_2 generation during the PEC process with SO_2 removal.

BiVO$_4$ moves faster than that produced in BiVO$_4$, and shows a significantly increased photocurrent density (**Figure 4**) and rate of H$_2$ production (**Figure 5**). The reactions are summarized as following:
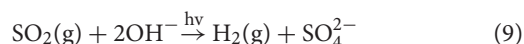
$$SO_2(g) + OH^- \rightarrow HSO_3^- \qquad (5)$$

$$HSO_3^- + OH^- \rightarrow SO_3^{2-} + H_2O \qquad (6)$$
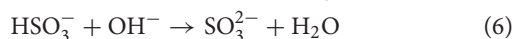
Reaction on photoanode (Mo-doped BiVO$_4$ film):

$$SO_3^{2-} + 2OH^- \rightarrow SO_4^{2-} + H_2O + 2e^- \qquad (7)$$

Reaction on cathode (Pt wire):

$$2H_2O + 2e^- \rightarrow H_2(g) + 2OH^- \qquad (8)$$
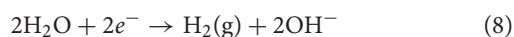
The total reaction:

$$SO_2(g) + 2OH^- \xrightarrow{h\nu} H_2(g) + SO_4^{2-} \qquad (9)$$

CONCLUSIONS

In summary, the effect of Mo doping on BiVO$_4$ used as photoanode for H$_2$ production with simultaneously flue gas SO$_2$ removal is investigated. The 3 atom% Mo-doped BiVO$_4$ (BiVO$_4$(Mo-3)) possessed the best PEC activity due to its better charge carrier transportation. With the help of Mo, the H$_2$ evolution rate and SO$_2$ removal rate of Mo-doped BiVO$_4$ almost 3 times higher than pristine BiVO$_4$. Through this process, the SO$_2$ in flue gas is removed and collected to produce H$_2$, which could greatly reduce the cost of desulfurization process, and even make it profitable.

AUTHOR CONTRIBUTIONS

JH: assisted in design of the experiments and wrote the manuscript; KL: performed the experiments and wrote the manuscript; HC: assisted in the analysis and interpretation of the data; LZ: planned the project, designed the experiments, and also wrote the manuscript.

ACKNOWLEDGMENTS

REFERENCES

Bashikova, S., Bagreev, A., Locke, D. C., and Bandosz, T. J. (2001). Adsorption of SO$_2$ on sewage sludge-derived materials. *Environ. Sci. Technol.* 35, 3263–3269. doi: 10.1021/es010557u

Berglund, S. P., Rettie, A. J., Hoang, S., and Mullins, C. B. (2012). Incorporation of Mo and W into nanostructured BiVO$_4$ films for efficient photoelectrochemical water oxidation. *Phys. Chem. Chem. Phys.* 14, 7065–7075. doi: 10.1039/c2cp40807d

Chen, L., Toma, F. M., Cooper, J. K., Lyon, A., Lin, Y. J., Sharp, I. D., et al. (2015). Mo-Doped BiVO$_4$ photoanodes synthesized by reactive sputtering. *ChemSusChem* 8, 1066–1071. doi: 10.1002/cssc.201402984

Ding, K. N., Chen, B., Fang, Z. X., Zhang, Y. F., and Chen, Z. F. (2014). Why the photocatalytic activity of Mo-doped BiVO$_4$ is enhanced: a comprehensive density functional study. *Phys. Chem. Chem. Phys.* 16, 13465–13476. doi: 10.1039/c4cp01350f

Han, J., Zheng, X. Z., Zhang, L. W., Fu, H. B., and Chen, J. M. (2017). Removal of SO$_2$ on a nanoporous photoelectrode with simultaneous H$_2$ production. *Environ. Sci. Nano* 4, 834–842. doi: 10.1039/C6EN00638H

Hong, S. J., Lee, S., Jang, J. S., and Lee, J. S. (2011). Heterojunction BiVO$_4$/WO$_3$ electrodes for enhanced photoactivity of water oxidation. *Energy Environ. Sci.* 4, 1781–1787. doi: 10.1039/c0ee00743a

Huang, H., Li, X., Wang, J., Dong, F., Chu, P. K., Zhang, T., et al. (2015). Anionic group self-doping as a promising strategy: band-gap engineering and multi-functional applications of high-performance CO$_3^{2-}$-doped Bi$_2$O$_2$CO$_3$. *ACS Catal.* 5, 4094–4103. doi: 10.1021/acscatal.5b00444

Huang, H., Tu, S., Zeng, C., Zhang, T., Reshak, A. H., and Zhang, Y. (2017). Macroscopic polarization enhancement promoting photo- and piezoelectric-induced charge separation and molecular oxygen activation. *Angew. Chem. Int. Ed.* 56, 11860–11864. doi: 10.1002/anie.201706549

Huang, H. W., He, Y., Du, X., Chu, P. K., and Zhang, Y. H. (2015). A General and facile approach to heterostructured core/shell BiVO$_4$/BiOI p-n junction: room-temperature *in situ* assembly and highly bootsed visible-light photocatalysis. *ACS Sustain. Chem. Eng.* 3, 3262–3273. doi: 10.1021/acssuschemeng.5b01038

Jiang, G., Lan, M., Zhang, Z., Lv, X., Lou, Z., Xu, X., et al. (2017). Identification of active hydrogen species on palladium nanoparticles for an enhanced electrocatalytic hydrodechlorination of 2,4-dichlorophenol in water. *Environ. Sci. Technol.* 51, 7599–7605. doi: 10.1021/acs.est.7b01128

Jiang, G. M., Zhu, H. Y., Zhang, X., Shen, B., Wu, L. H., Zhang, S., et al. (2015). Core/Shell face-centered tetragonal FePd/Pd nanoparticles as an efficient non-Pt catalyst for the oxygen reduction reaction. *ACS Nano* 9, 11014–11022. doi: 10.1021/acsnano.5b04361

Jo, W. J., Jang, J. W., Kong, K. J., Kang, H. J., Kim, J. Y., Jun, H., et al. (2012). Phosphate doping into monoclinic BiVO$_4$ for enhanced photoelectrochemical water oxidation activity. *Angew. Chem. Int. Ed.* 51, 3147–3151. doi: 10.1002/anie.201108276

Kaplan, V., Wachtel, E., and Lubomirsky, I. (2013). Carbonate melt regeneration for efficient capture of SO$_2$ from coal combustion. *RSC Adv.* 3, 15842–15849. doi: 10.1039/c3ra42654h

Kim, T. W., and Choi, K. S. (2014). Nanoporous BiVO$_4$ photoanodes with dual-layer oxygen evolution catalysts for solar water splitting. *Science* 343, 990–994. doi: 10.1126/science.1246913

Kuang, Y. B., Jia, Q. X., Ma, G. J., Hisatomi, T., Minegishi, T., Nishiyama, H., et al. (2016). Ultrastable low-bias water splitting photoanodes via photocorrosion inhibition and *in situ* catalyst regeneration. *Nat. Energy* 2:16191. doi: 10.1038/nenergy.2016.191

Lelieveld, J., and Heintzenberg, J. (1992). Sulfate cooling effect on climate through in-colud oxidation of anthropogenic SO$_2$. *Science* 258, 117–120.

Lu, Z. F., Streets, D. G., Foy, B., and Krotkov, N. A. (2013). Ozone monitoring instrument observations of interannual increases in SO$_2$ emissions from indian coal-fired power plants during 2005-2012. *Environ. Sci. Technol.* 47, 13993–14000. doi: 10.1021/es4039648

Luo, W. J., Wang, J. J., Zhao, X., Zhao, Z. Y., Liab, Z. S., and Zou, Z. G. (2013). Formation energy and photoelectrochemical properties of BiVO$_4$ after doping at Bi^{3+} or V^{5+} sites with higher valence metal ions. *Phys. Chem. Chem. Phys.* 15, 1006–1013. doi: 10.1039/C2CP43408C

Luo, W. J., Yang, Z. S., Li, Z. S., Zhang, J. Y., Liu, J. G., Zhao, Z. Y., et al. (2011). Solar hydrogen generation from seawater with a modified BiVO$_4$ photoanode. *Energy Environ. Sci.* 4, 4046–4051. doi: 10.1039/c1ee01812d

McDonald, K. J., and Choi, K. S. (2012). A new electrochemical synthesis route for a BiOI electrode and its conversion to a highly efficient porous BiVO$_4$

photoanode for solar water oxidation. *Energy Environ. Sci.* 5, 8553–8557. doi: 10.1039/c2ee22608a

McDonald-Buller, E., Kimura, Y., Craig, M., McGaughey, G., Allen, D., and Webster, M. (2016). Dynamic management of NO_x and SO_2 emissions in the texas and Mid-Atlantic electric power systems and implications for air quality. *Environ. Sci. Technol.* 50, 1611–1619. doi: 10.1021/acs.est.5b04175

Nair, V., Perkins, C. L., Lin, Q. Y., and Law, M. (2016). Textured nanoporous Mo:$BiVO_4$ photoanodes with high charge transport and charge transfer quantum efficiencies for oxygen evolution. *Energy Environ. Sci.* 9, 1412–1429. doi: 10.1039/C6EE00129G

Park, Y., Kang, D., and Choi, K. S. (2014). Marked enhancement in electron-hole separation achieved in the low bias region using electrochemically prepared Mo-doped $BiVO_4$ photoanodes. *Phys. Chem. Chem. Phys.* 16, 1238–1246. doi: 10.1039/C3CP53649A

Parmar, K. P. S., Kang, H. J., Bist, A., Dua, P., Jang, J. S., and Lee, J. S. (2012). Photocatalytic and photoelectrochemical water oxidation over metal-doped monoclinic $BiVO_4$ photoanodes. *ChemSusChem* 5, 1926–1934. doi: 10.1002/cssc.201200254

Pattengale, B., and Huang, J. (2016). The effect of Mo doping on the charge separation dynamics and photocurrent performance of $BiVO_4$ photoanodes. *Phys. Chem. Chem. Phys.* 18, 32820–32825. doi: 10.1039/C6CP06407H

Pilli, S. K., Furtak, T. E., Brown, L. D., Deutsch, T. G., Turner, J. A., and Herring, A. M. (2011). Cobalt-phosphate (Co-Pi) catalyst modified Mo-doped $BiVO_4$ photoelectrodes for solar water oxidation. *Energy Environ. Sci.* 4, 5028–5034. doi: 10.1039/c1ee02444b

Seabold, J. A., and Choi, K. S. (2012). Efficient and stable photo-oxidation of water by a bismuth vanadate tPhotoanode coupled with an iron oxyhydroxide oxygen evolution catalyst. *J. Am. Chem. Soc.* 134, 2186–2192. doi: 10.1021/ja209001d

Seabold, J. A., Zhu, K., and Neale, N. R. (2014). Efficient solar photoelectrolysis by nanoporous Mo:$BiVO_4$ through controlled electron transport. *Phys. Chem. Chem. Phys.* 16, 1121–1131. doi: 10.1039/C3CP54356K

Srinivasan, A., and Grutzeck, M. W. (1999). The adsorption of SO_2 by zeolites synthesized from fly ash. *Environ. Sci. Technol.* 33, 1464–1469. doi: 10.1021/es9802091

Thalluri, S. M., Hernández, S., Bensaid, S., Saracco, G., and Russo, N. (2016). Green-synthesized W- and Mo-doped $BiVO_4$ oriented along the {040} facet

with enhanced activity for the sun-driven water oxidation. *Appl. Catal. B Environ.* 180, 630–636. doi: 10.1016/j.apcatb.2015.07.029

Xia, D. H., He, C., Zhu, L. F., Huang, Y. L., Dong, H. Y., Su, M. H., et al. (2011). A novel wet-scrubbing process using Fe(VI) for simultaneous removal of SO_2 and NO. *J. Environ. Monit.* 13, 864–870. doi: 10.1039/c0em00647e

Yang, Z. Z., He, L. N., Song, Q. W., Chen, K. H., Liu, A. H., and Liu, X. M. (2012). Highly efficient SO_2 absorption/activation and subsequent utilization by polyethylene glycol-functionalized Lewis basic ionic liquids. *Phys. Chem. Chem. Phys.* 14, 15832–15839. doi: 10.1039/c2cp43362a

Yang, Z. Z., He, L. N., Zhao, Y. N., and Yu, B. (2013). Highly efficient SO_2 absorption and its subsequent utilization by weak base/polyethylene glycol binary system. *Environ. Sci. Technol.* 47, 1598–1605. doi: 10.1021/es304147q

Zhang, L. W., Lin, C. Y., Valev, V. K., Reisner, E., Steiner, U., and Baumberg, J. J. (2014). Plasmonic enhancement in $BiVO_4$ photonic crystals for efficient water splitting. *Small* 10, 3970–3978. doi: 10.1002/smll.201400970

Zhang, L., Ye, X., Boloor, M., Poletayev, A., Melosh, N. A., and Chueh, W. C. (2016). Significantly enhanced photocurrent for water oxidation in monolithic Mo:$BiVO_4$/SnO_2/Si by thermally increasing the minority carrier diffusion length. *Energy Environ. Sci.* 9, 2044–2052. doi: 10.1039/C6EE00036C

Zhou, M., Bao, J., Xu, Y., Zhang, J. J., Xie, J. F., Guan, M. L., et al. (2014). Photoelectrodes based upon Mo: $BiVO_4$ inverse opals for photoelectrochemical water splitting. *ACS Nano* 8, 7088–7098. doi: 10.1021/nn501996a